

The Dynamics, Destruction, and Survival of Supernova-Formed Dust Grains

JONATHAN D. SLAVIN ¹, ELI DWEK ², MORDECAI-MARK MAC LOW ^{3,4} AND
ALEX S. HILL ^{5,6,7}

¹*Center for Astrophysics | Harvard & Smithsonian, 60 Garden Street, Cambridge, MA 02138, USA*

²*Observational Cosmology Lab, NASA Goddard Space Flight Center, Mail Code 665, Greenbelt, MD 20771, USA*

³*American Museum of Natural History, 79th Street at Central Park West, New York, NY 10024, USA*

⁴*Center for Computational Astrophysics, Flatiron Institute, New York, NY, 10010, USA*

⁵*Space Science Institute, Boulder, CO 80301, USA*

⁶*Department of Computer Science, Math, Physics, and Statistics, University of British Columbia, Okanagan Campus, 3187 University Way, Kelowna, BC V1V 1V7 Canada*

⁷*Dominion Radio Astrophysical Observatory, Herzberg Program in Astronomy and Astrophysics, National Research Council Canada, Penticton, BC V2A 6J9 Canada*

ABSTRACT

Observations have demonstrated that supernovae efficiently produce dust. This is consistent with the hypothesis that supernovae and asymptotic giant branch stars are the primary producers of dust in the Universe. However, there has been a longstanding question of how much of the dust detected in the interiors of young supernova remnants can escape into the interstellar medium. We present new hydrodynamical calculations of the evolution of dust grains that were formed in dense ejecta clumps within a Cas A-like remnant. We follow the dynamics of the grains as they decouple from the gas after their clump is hit by the reverse shock. They are subsequently subject to destruction by thermal and kinetic sputtering as they traverse the remnant. Grains that are large enough ($\sim 0.25 \mu\text{m}$ for silicates and $\sim 0.1 \mu\text{m}$ for carbonaceous grains) escape into the interstellar medium while smaller grains get trapped and destroyed. However, grains that reach the interstellar medium still have high velocities, and are subject to further destruction as they are slowed down. We find that for initial grain size distributions that include large ($\sim 0.25 - 0.5 \mu\text{m}$) grains, 10–20% of silicate grains can survive, while 30–50% of carbonaceous grains survive even when the initial size distribution cuts off at smaller ($0.25 \mu\text{m}$) sizes. For a $19 M_{\odot}$ star similar to the progenitor of Cas A, up to $0.1 M_{\odot}$ of dust can survive if the dust grains formed are large. Thus we show that supernovae under the right conditions can be significant sources of interstellar dust.

Keywords: Interstellar dust, Interstellar dust processes, Supernova remnants

1. INTRODUCTION

Dust plays a variety of important roles in the interstellar medium (ISM) in a wide array of environments. In low-density warm and cold neutral regions it can be an important source of heat via photoelectric emission (e.g. [Wolfire et al. 2003](#), and references therein). In molecular clouds dust is important as a site for molecule formation (e.g. [Hollenbach & Salpeter 1971](#)), as well as shielding molecules from ultraviolet radiation, and cooling the gas at the highest densities. Dust can also be an important coolant for hot gas via conversion of thermal energy to infrared (IR) emission ([Dwek 1987](#)). As a repository of metals, dust regulates the gas phase abundances and metal transport in galaxies.

The evolution of dust is complex and is driven by many of the key processes involved in galactic evolution. The cores of dust grains are known to form in the dense ejecta of supernovae (SNe) and in the slow, dense winds from evolved stars, especially asymptotic giant branch stars. Interstellar grains are destroyed primarily by sputtering, which is enhanced behind shock waves because of the presence of high pressure hot gas or, in radiative shocks, high compression, which leads to betatron acceleration and accompanying inertial sputtering and grain-grain collisions (which shatter grains, changing the size distribution). Thus grain destruction is tightly coupled to the rate of energy injection into the ISM by SNe. The persistent problem of the apparent imbalance of grain destruction rates and creation rates (see e.g. [Jones et al. 1994](#)) has led to the idea that accretion of gas onto pre-existing grain cores is important to maintaining the levels of gas phase depletion inferred for the ISM ([Draine & Salpeter 1979a](#); [Dwek & Scalo 1980](#); [Draine 2009](#)). While such accretion could be the solution to the grain destruction problem, it is nonetheless important that grain cores are injected at an adequate rate since it does not appear to be possible to create such cores in the ISM.

SNe are known creators of dust as has been shown directly by infrared (IR) observations ([Barlow et al. 2010](#); [Gomez et al. 2012](#); [Arendt et al. 2014](#); [Matsuura et al. 2015](#)). The most notable dust sources are SN 1987A, Cas A, The Crab Nebula and G54.1+0.3. A more complete list of Galactic and extragalactic sources can be found in [Sarangi et al. \(2018\)](#). In particular far-IR observations, for example with Herschel, have shown that remnants such as Cas A and SN 1987A have created $\sim 1 M_{\odot}$ of dust in the densest regions of their ejecta. This dust, however, is cold and has not yet encountered the reverse shock that will eventually heat the interior of the remnants to very high temperatures and may destroy significant amounts of the newly created dust ([Dwek 2005](#)). Though it is known that some dust created in SNe does escape, e.g. based on the isotopes found in some pre-solar grains in meteorites (e.g. [Hoppe et al. 2015](#)), whether or not SNe are important sources of interstellar dust in

the present-day universe remains uncertain. There is also keen interest in whether SNe in high-redshift galaxies can produce the high levels of dust observed in them (Bertoldi et al. 2003; Gall et al. 2011; Dwek & Cherchneff 2011), since in many cases the galaxies are too young for stars to have evolved to the AGB phase.

There have been several studies of the question of the survival of dust formed in SNe (Dwek 2005; Nozawa et al. 2007; Bianchi & Schneider 2007; Nath et al. 2008; Silvia et al. 2012, 2010; Biscaro & Cherchneff 2016; Micelotta et al. 2016; Bocchio et al. 2016; Kirchschrager et al. 2019), mainly focused on how much destruction occurs when the reverse shock sweeps over the newly formed grains. These studies have used a range of methods and made predictions ranging from very low destruction to complete destruction of the dust. Of these previous studies, the ones that have employed hydrodynamical calculations (Silvia et al. 2010, 2012; Kirchschrager et al. 2019) have all used a plane parallel shock encountering a cloud, or ejecta clump. Those previous works have examined how much grain destruction occurs due to sputtering when the clump is shocked and heated. Silvia et al. (2012) assumed that the grains were tightly coupled to the gas and that thermal sputtering was the dominant process. Micelotta et al. (2016) took a different approach, examining how grains in the clumps get sputtered when they decouple from the gas and stream out of the clump as it is decelerated by the reverse shock. Kirchschrager et al. (2019) included more processes, including inertial sputtering, grain-grain collisions and decoupling of the gas and dust. They treat the dust in post-processing using what they term a dusty-grid approach. This approach amounts to a multi-fluid treatment because, though the dust can move relative to the gas, grains from one grid zone cannot interpenetrate those from a different grid zone and grains from each zone all move together. We discuss these assumptions further below. These studies are important since they have demonstrated that substantial grain destruction can occur when the reverse shock hits an ejecta clump. However, grains that survive the reverse shock are still within the hot gas of the evolving SN remnant and thus subject to continued sputtering.

Determining if grains escape the SN remnant requires tracking the motion of the grains relative to the shock front in the evolving remnant. In this paper we present results from new hydrodynamical calculations in which we track the grains as they evolve with the remnant. We simulate a remnant that is similar to Cas A including very small and high density ejecta clumps. We start our simulations with grains inside the clumps and follow the dust trajectories as they are sputtered because of their interaction with the gas and suffer drag when they have substantial velocity relative to the surrounding gas. We follow the grains until they either escape the remnant or are destroyed. Escaping grains are further destroyed while being slowed in the ISM. Our results are important for assessing under which conditions grains can fully escape the SN remnant to enter the general ISM and thus the rate at which SNe can supply dust to the ISM.

The survival of the dust depends on the morphology of the SN ejecta, and that of the ambient medium of the progenitor star. To simulate a realistic scenario we have created models that use the Cassiopeia A SN remnant as an example. That is to say, we use the observations of Cas A to guide our parameter choices while not attempting to match the remnant in detail. Thus, for example, we use clumpy ejecta that are roughly of the size determined for those in Cas A. On the other hand we make no attempt to model the jet or the complex abundance variations that are seen in Cas A. Our goal is to focus on aspects of the remnant that have the most impact on the evolution of the dust generated within the remnant. Our overall aim has been to create models that may be widely applicable to core-collapse SN remnants that produce dust.

2. METHODS

2.1. *Hydrodynamical Simulations*

For the hydrodynamical simulations presented here we have used the publicly available and well-tested FLASH code¹ (Fryxell et al. 2000; Dubey et al. 2012). Because of the need for very high dynamic range in order to resolve the ejecta clumps, $R_{\text{clump}} \sim 10^{16}$ cm (Fesen et al. 2011), while following the remnant evolution to relatively large size, ~ 20 pc, we have run our simulations in two dimensions (2D) with cylindrical symmetry. We have made use of FLASH’s adaptive mesh refinement capabilities with eight levels of refinement, which leads to a resolution at full refinement of 7.53×10^{15} cm (0.00244 pc). For our grid, which extends from 0 to 20 pc in r and -20 to $+20$ pc in z , this would be, if fully refined, 8192×16384 zones.

Dust grains in the ISM are coupled to the gas via drag forces and the magnetic field. We have not included the magnetic field in our calculations for reasons that we discuss below. We have included both drag and sputtering (grain erosion) and have allowed for the independent motion of individual grains. The FLASH code provides units for following both active and passive particles where the former act on the gas (by gravitational force in the provided unit) and are free to move independently of the gas while the latter simply move with the gas acting as Lagrangian tracers. Evolution of the particle mass is not included in the active particle unit. Dust does not fit neatly into either category since typically it does not include enough mass to significantly affect the gas dynamics and yet couples only imperfectly to the gas via drag (and the magnetic field) and can thus move independently of the gas. For this reason we needed to develop our own unit that builds on the existing active particle unit. We also developed a short range force unit that implements gas drag as well as sputtering.

Another modification to the basic code base of FLASH that we have made is to add radiative cooling via a lookup table. Our approach has been similar to that

¹ <http://flash.uchicago.edu/site/flashcode/>

in the user-contributed supplemental SutherlandDopita (Sutherland & Dopita 1993) unit (under `physics/sourceTerms/Cool`) though it differs in detail. The table of cooling coefficients we have used was generated by us using the code Cloudy. We ran Cloudy (Ferland et al. 2017, version 17.00) as a subroutine using abundances like those inferred for the O-rich ejecta in Cas A (essentially pure O) over a large range of temperatures. This cooling curve would not be appropriate for the smooth ejecta nor for the circumstellar medium or ISM around the remnant. However, this is not a problem for our simulations, since cooling is unimportant in those regions over the time span of our simulations because of their low densities.

2.2. Initial Conditions

We initiate our simulations with fast-expanding ejecta that contain embedded dense clumps. The ejecta initially have a constant density core with density of the smooth ejecta of $\rho_{sm} = 3.831 \times 10^{-23} \text{ g cm}^{-3}$. Outside of the core is the envelope in which the density declines steeply, $\rho \propto r^{-9}$. (Note that here and in our discussion below regarding the progenitor stellar wind region, r is the spherical distance from the origin, not the cylindrical distance from the symmetry axis.) The clumps are a factor of 100 times denser than the surrounding smooth ejecta with initial radii of 3×10^{16} cm. This is somewhat larger than observed, though the observations are of clumps that have been shocked and compressed. The clumps are in pressure equilibrium with the ejecta, though this does not matter much since the thermal energy is very small compared to the kinetic energy. They are limited to the smooth ejecta region initially and their number is set by our assumed volume filling factor for the clumps of 2%. For our assumed parameters this leads to 61 clumps, which are scattered randomly within the ejecta core and are sharp edged circles (tori in cylindrical symmetry). The mean density in the core is $\langle \rho_{core} \rangle = ((1 - f_{cl}) + \chi f_{cl}) \rho_{sm}$ where f_{cl} is the clump filling factor, χ is the ratio of clump density to smooth density (100 in our calculations) and ρ_{sm} is the density of the smooth ejecta. For our assumptions, $\langle \rho_{core} \rangle = 1.141 \times 10^{-22} \text{ g cm}^{-3}$. For the purposes of calculating the cooling in the clumps, they are assumed to be essentially pure oxygen (see discussion below). The initial velocity profile is assumed to be linear, $v \propto r$, from the origin to the edge of the ejecta envelope. Our assumed initial density profile is shown in figure 1, though without the dense clumps.

The combination of our assumed ejecta mass, $3.5 M_{\odot}$, explosion energy, 1.5×10^{51} ergs, and maximum speed, 9000 km s^{-1} , along with the mean density in the ejecta core, fix the size of the core relative to outer edge of the ejecta envelope. In our case that ratio is 0.919. With our assumed ejecta radius of 0.85 pc, this makes the radius of the core 0.78 pc. The dust grain particles in the simulations are all started randomly scattered inside the dense clumps. We have used 40 grains per clump in results presented here. We have carried out separate runs for each grain size and type discussed. All grains start with the same size for a given run.

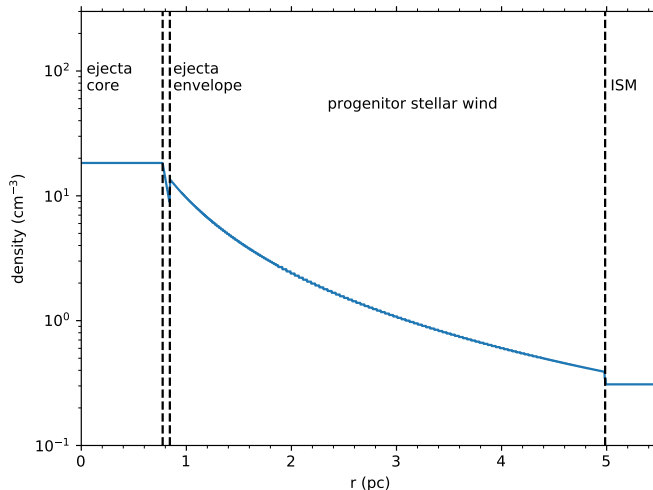


Figure 1. Initial density profile for our simulations. In this 1D rendering the dense ejecta clumps are not included. Note that here r is the radial distance from the explosion center, not the cylindrical distance from the z axis.

Outside of the ejecta envelope we assume a circumstellar medium density declining as $\rho \propto r^{-2}$, under the assumption that the explosion occurred in the stellar wind-blown bubble of the progenitor. There are observational constraints on the density of the circumstellar medium at the current location of the forward shock, $R_b \approx 2.5$ pc (Willingale et al. 2003; Lee et al. 2014), but the constraints are not tight. We found that the value of 2.07 cm^{-3} in Micelotta et al. (2016) was too high to allow for the forward shock to reach $R_b \approx 2.5$ pc by ~ 330 yr. In addition, the total mass in the circumstellar bubble would be very high unless the bubble were quite small. We can connect the parameters of the circumstellar bubble with the stellar parameters and observed characteristics of the remnant by using a combination of the density at the (current) forward shock, the progenitor mass and the ejecta mass. For this we have assumed that the progenitor of Cas A was a $19 M_{\odot}$ star, that the mass of shocked circumstellar medium inside of R_b is $6.2 M_{\odot}$, and the ejecta mass was $3.5 M_{\odot}$. This leads to a density at 2.5 pc of 1.5 cm^{-3} , which is roughly consistent with Lee et al. (2014), who found a density at the forward shock of $\sim 1 \text{ cm}^{-3}$. With our choice of parameters, the bubble extends to 5 pc, outside of which we assumed a constant density ISM with $n = 0.309 \text{ cm}^{-3}$.

2.3. Extrapolating Grain Evolution

In Section 3, we present simulation results for a time of 8000 yr. While that allowed for grains to escape ahead of the SN remnant shock in some cases, in other cases the grains remain inside the shock. In either case the question of the final state of a grain when its speed finally drops below the sputtering threshold in the ambient ISM remains undetermined. Thus we have found it necessary to extrapolate the evolution of the grains.

The extrapolation that we have performed has two parts. First, we used the radially averaged profiles of pressure, density and radial velocity from the final time step of the 2D simulation to initiate a one-dimensional (1D; spherically symmetric) simulation that we ran on a large (50 pc) grid for 10^5 yr. That allowed us to calculate the shock radius as a function of time. With the assumption that the fluid variables follow a Sedov-Taylor type similarity solution (see e.g. Cox & Franco 1981), we can use the time evolution of the shock radius to find values of density, temperature, and gas velocity for locations inside the remnant for late times. We have compared such profiles with the 1D simulation profiles and found the match very good in the outer regions of the remnant where the dust is concentrated at late times. For the 1D simulation, we included radiative cooling with a cooling curve appropriate for solar abundances. With this cooling, the remnant only starts to go radiative at about 7×10^4 yr. After this point the Sedov-Taylor profile no longer provides a good approximation to the radial profiles of the fluid variables and we stop the extrapolation.

We used the 1D extrapolated remnant evolution in conjunction with the equations for drag on the grains and thermo-kinetic sputtering (see §2.4) to calculate the motion and mass evolution of the grains beyond the 8000 yr endpoint of our 2D simulations. In fact for runs with large initial grain sizes, some of the grains leave the grid before the end of the simulation. For those grains we use their last position and speed to extrapolate their evolution. In general the vast majority of the grains have either been effectively completely destroyed ($m/m(0) < 0.005$) or have fully escaped the remnant such that they are beyond the shock and have speeds that exceed the shock speed when we stop the extrapolation at $t = 7 \times 10^4$ yr. There are typically a small number of grains that have not fully escaped the remnant but appear likely to do so. These are grains that started close to the explosion site such that their initial velocity was relatively low. Some complex behaviors are seen, such as grains that get ahead of the shock but are then caught by the shock after getting slowed by drag in the ISM. Also, even grains that have fully escaped the remnant, cannot be considered to be part of the ISM until they slow to below the sputtering threshold speed, which we calculate to be $v_{\text{thresh}} \approx 20 \text{ km s}^{-1}$. For that reason we further extrapolate the grain evolution past the cooling time of the 1D simulation at 7×10^4 yr, using the results as plotted in Figure 2 to calculate the further reduction of mass that will result as the grains are slowed below v_{thresh} .

2.4. Grain Processing

Grain sputtering is caused by gas atoms and ions colliding with dust grains with enough energy to knock atoms off the grain. When the relative speed of the grain to the gas is much less than the thermal speed of the gas particles (typically hot gas, $T \gtrsim 10^6$ K) then sputtering is primarily thermal since the velocity distribution of incident particles is Maxwellian. If the grain speed is large compared to the thermal speeds (typically cold gas, $T \lesssim 10^4$ K), the sputtering is referred to as inertial (or

kinetic), since the velocity distribution of the incident particles is determined by the relative velocity of the grains through the gas. In the general case, both the thermal speed of the particles and the gas-grain velocity are important. In that case the sputtering rate depends on the yield integrated over a Maxwellian particle distribution skewed by the gas-grain relative velocity and so depends on both the gas temperature and the relative velocity. Thus the sputtering rate is

$$\frac{dm_{gr}}{dt} = -\pi a_{gr}^2 m_{sp} n_H \sum_i A_i \langle Y(E_i) v \rangle \quad (1)$$

where $\langle Yv \rangle$ is the yield times the relative gas-grain speed integrated over the velocity distribution function of the gas particles in the frame of the grain (typically a skewed Maxwellian), m_{sp} is the average mass of a sputtered atom, n_H is the number density of H in the gas, A_i is the gas phase abundance of gas particle i and the sum is over incident gas particle types (i.e. elements). The skewed Maxwellian speed distribution can be expressed as

$$f(v, v_{gr}, T) = \sqrt{\frac{m}{2\pi kT}} \left(\frac{v}{v_{gr}}\right) \left(\exp\left(-\frac{m(v - v_{gr})^2}{2kT}\right) - \exp\left(-\frac{m(v + v_{gr})^2}{2kT}\right)\right) \quad (2)$$

when the integration is over speed (see, e.g. [Dwek & Arendt 1992](#)). Note that $Y(E_i)$ above is the angle integrated value rather than the normal incidence value for the yield. We have used the yields from [Nozawa et al. \(2006\)](#), which are based on [Tielens et al. \(1994\)](#), adopting the values for MgSiO₃ for the silicate grains and those for amorphous C for the carbonaceous grains. To ease the computational burden that would be required to calculate the integral for each grain and time step, we have created tables of $\langle Yv \rangle$ for a large range of temperatures and grain speeds relative to the gas and for each grain type (carbonaceous and silicate) and incident atom type (including H, He, C and O). The tables are read in during initialization and values of $\langle Yv \rangle$ are found through interpolation to calculate the sputtering rate during the simulations.

We include the effects of drag on the grains as well, which is essential to calculating their evolution. The grain velocity evolves as

$$\frac{d\mathbf{v}_{gr}}{dt} = \frac{-\pi a_{gr}^2 \rho_{gas}}{m_{gr}} \xi(\mathbf{v}_{gr} - \mathbf{v}_{gas}) |\mathbf{v}_{gr} - \mathbf{v}_{gas}|, \quad (3)$$

where a_{gr} is the grain radius, m_{gr} is the grain mass, \mathbf{v}_{gr} is the grain velocity, \mathbf{v}_{gas} is the gas velocity and

$$\xi = \left(1 + \frac{128}{9\pi} \frac{kT}{mv^2}\right)^{1/2} \quad (4)$$

([Baines et al. 1965](#); [Draine & Salpeter 1979b](#)). Here v is the absolute value of the relative gas-grain speed and T is the gas temperature. We note that we have ignored the plasma drag. As we discuss further below, we have found it is small compared

with the direct drag for the conditions in our simulations. Ignoring the plasma drag relieves us of the need to calculate the grain charge, which would involve significant additional computational overhead.

2.4.1. Grain Slowing in the ISM

As discussed above, to examine the remnant evolution over longer timescales, we used our 2D simulation results, radially averaged, to initiate a 1D simulation in a much larger grid (50 pc) for a time of 10^5 yr. From that simulation we derive the long term evolution of the shock size and speed in the, assumed uniform, ISM. However even at the end of the 1D simulation, most grains have not slowed enough in the ISM to have stopped sputtering.

Once the grains get into the uniform ISM, we can determine analytically how much more of their mass will be sputtered while they are slowed to a velocity below the sputtering threshold. As shown by [Micelotta et al. \(2016\)](#) this can be done by combining equations (1) and (3) to get

$$\frac{dm_{\text{gr}}}{dv_{\text{gr}}} = \frac{m_{\text{gr}}}{v_{\text{gr}}} \frac{m_{\text{sp}} n_{\text{H}}}{\rho_{\text{gas}} \xi} \sum_i A_i Y_i(E) \quad (5)$$

which can be solved to yield

$$\frac{m_{\text{gr}}(t)}{m_{\text{gr}}(0)} = \exp \left[\frac{m_{\text{sp}} n_{\text{H}}}{\rho_{\text{gas}} \xi} \int_{v_{\text{gr}}(0)}^{v_{\text{gr}}(t)} \sum_i A_i Y_i(E) \frac{dv_{\text{gr}}}{v_{\text{gr}}} \right], \quad (6)$$

where $E = m_i v_{\text{gr}}^2 / 2$. Here we are assuming that the sputtering is purely inertial since the ISM has a low enough temperature ($T \lesssim 10^4$ K) that thermal sputtering is not important. The ratio of final to initial mass that results for grains that are slowed below the sputtering threshold then only depends on the initial grain velocity relative to the gas, the grain type, and the gas composition. For our assumed grain types and interstellar gas composition (logarithmic gas phase abundances relative to H = 12: $A_{\text{He}} = 11.0$, $A_{\text{C}} = 8.31$, $A_{\text{N}} = 7.99$, $A_{\text{O}} = 8.83$) we get the curves plotted in Figure 2. Note that the destruction saturates effectively for very high speeds such that there is a maximum fraction of the initial mass that is sputtered. This happens because the yield curves turn over at high energy, because the grains become effectively transparent to the particles for high enough relative speeds.

2.4.2. Neglected Processes

We note that, while we believe that we have included all of the dominant processes in our calculations, other works have included some that we have left out. Most importantly we have not included the magnetic field which may significantly change the grains' trajectories, even possibly returning them to the remnant after they escape. It is unknown how strong the magnetic field is in SN ejecta. If it is just the stellar magnetic field diluted via expansion, it would be extremely small because the stellar

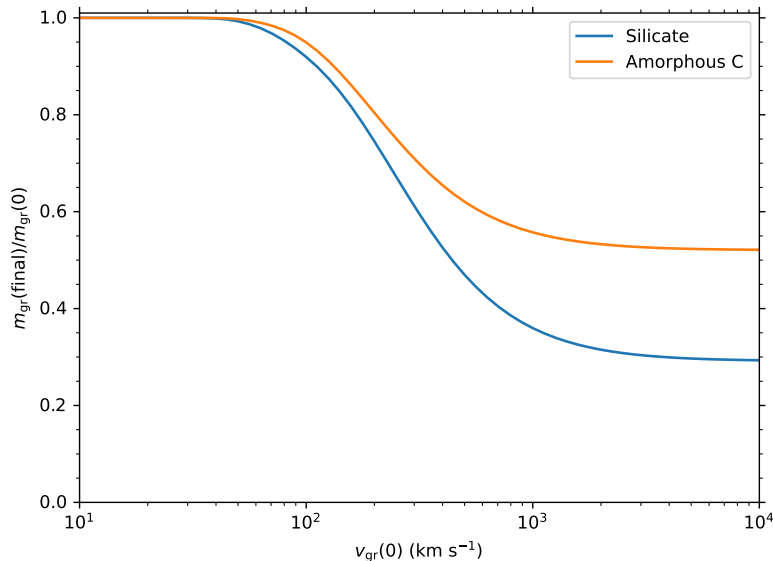


Figure 2. Final surviving grain mass fraction as a function of initial grain speed relative to the gas. The assumption here is that only inertial sputtering is important and depends on the assumed elemental composition of the medium. It is also implicitly assumed that the medium is uniform in temperature. The relation plotted allows us to extrapolate to find the surviving mass fraction of grains that reach, and are stopped in, the uniform ISM surrounding the SN that produced them.

dipole field will be diluted as the cube of the expansion radius. In the ISM it is quite likely that grains will encounter magnetic fields with typical magnitudes of several microgauss, which could be important for the trajectories of the grains. However, grains exiting the remnant at speeds of several hundreds to thousands of kilometers per second will have gyroradii large enough in most cases that they will not return to the remnant.

The charge that the grains will have at the low temperatures of the cold or warm ISM depends on the UV environment and electron density. As described in, for example [McKee et al. \(1987\)](#), the controlling parameter is proportional to G_0/n_e where G_0 is a measure of the FUV background. The grain speed also plays an important role. We have found that the gyroradii for grains escaping the remnant span a wide range from ~ 1 pc to hundreds of parsecs, depending on the parameter values assumed. In addition there is the question of the morphology of the magnetic field. A uniform field could allow for reflection of the grains back into the remnant, while a field with a turbulent component could allow for diffusion of the grains through the ISM. Recent work by [Fry et al. \(2020\)](#) finds that a large fraction of grains are reflected back into the remnant by the magnetic field. However that work focuses on Fe grains and they find grain charges that differ substantially from those that we find for the silicate and carbonaceous grains that we study in this paper. Given the uncertainties in the charging and the interstellar field we do not consider magnetic field in this work and only note that it could reduce the grain escape under particular sets of conditions.

Another process that we have neglected is grain-grain collisions. Inclusion of grain-grain collisions requires knowledge of the full population of grains in a region and their relative velocities, which is not feasible within the confines of our method of following grain trajectories. The results of grain-grain collisions include shattering, which redistributes grain mass from large grains to smaller ones, and vaporization, which destroys grains. For grains that are simply slowing in the ISM, shattering will have little effect on the total grain mass since smaller grains that are created will slow quickly and lose a fraction their mass determined by their velocity relative to the gas. Only vaporization will lead to excess mass loss. This contrasts with the situation for shocks propagating in the ISM (e.g. Jones et al. 1996; Slavin et al. 2015). For fast shocks in the ISM, $v_{\text{shock}} \gtrsim 150 \text{ km s}^{-1}$, shattering creates small grains that are thermally sputtered faster than the equivalent mass in larger grains during the short period in the post-shock flow that the gas is hot enough for thermal sputtering to be important. For slower shocks, although grain-grain collisions dramatically change the grain size distribution, the effect on grain destruction is minor because the hot post-shock zone is very thin. Thus we believe that for SN grains that are stopped in the ISM, grain-grain collisions may change their size distribution but will not affect the total mass in dust substantially.

For grains propagating in the hot shocked region of the SNR before escaping into the ISM, grain-grain collisions could occur where larger grains from deeper in the remnant collide with smaller grains that were slowed closer to the forward shock. The relatively large volume of the hot shocked region means that the volume density of grains will be small and the probability of collisions low. The high densities in the ejecta clumps and their possibly low gas-to-dust ratios provide a more likely scenario for grain-grain collisions being important. Since the grains begin moving outward together, we do not expect them to have substantial speeds relative to each other in general. (We assume that there has been no dust formed in the smooth ejecta because of the much lower density there.) With ejecta clumps that are further out moving faster initially, we do not see much passing of the farther out grains by those interior to them. Nevertheless, especially in clumps that contain a range of grain sizes, it is possible that a significant number of collisions could occur between slowed small grains and large grains which would tend to decrease the average grain size and reduce grain survival. Kirchschrager et al. (2019) have included grain-grain collisions in their calculations and find them to have a significant impact on grain destruction, though their calculations differ from ours in several ways.

A newly proposed process that we also do not include is grains growth via implantation (or ion trapping) of heavy ions into the grains Kirchschrager et al. (2020). This could increase the grain size in the ejecta clumps before the grains escape into the ISM. However, since the initial grain size distribution and the condensation efficiency in the ejecta is quite uncertain (see §3) one could consider those effects to be folded into that uncertainty.

Finally, we do not include plasma drag in our calculations. Plasma drag depends on the grain charge and several characteristics of the plasma,

$$F_d = 4\pi a^2 k_B T \phi^2 \ln \Lambda \sum_i n_i z_i^2 H(s_i), \quad (7)$$

where a is the grain size, T is the plasma temperature, $\phi = Ze^2/ak_B T$ is the potential parameter, $\ln \Lambda$ is the Coulomb logarithm, and the sum is over elements in the gas phase. See [McKee et al. \(1987\)](#) and references therein for details. We have carried out calculations of the grain charge, as we did in [Slavin et al. \(2015\)](#) using methods from [Weingartner & Draine \(2001\)](#) with updates from [Weingartner et al. \(2006\)](#) and modifications to include the relative gas-grain velocity. Exploring a variety of conditions like those that the grains in our simulations are subject to, we find that the plasma drag is very small compared with the gas drag in all cases.

3. RESULTS

Our simulated remnants evolve in the familiar way with a forward shock forming, a reverse shock propagating backward (relative to the expanding ejecta), and a contact discontinuity separating the shocked ejecta from the shocked circumstellar medium. However, because of their high density, the ejecta clumps decelerate more slowly than the smooth ejecta. Thus after the reverse shock passes a clump, the shocked smooth ejecta sweeps past it in the clump frame, leading to a shear flow. This drives turbulence in the shocked ejecta and the clump, producing a complex velocity field that affects grain trajectories as the grains escape their natal clumps. The fastest clumps that start farthest from the explosion center quickly cross the contact discontinuity and propagate into the shocked circumstellar medium, which disrupts and smears the contact discontinuity. The reverse shock speed starts at about 5000 km s^{-1} but then drops to around 2000 km s^{-1} , a bit higher than the observed value of $1000 - 2000 \text{ km s}^{-1}$ derived from observations of Cas A ([Laming & Hwang 2003](#); [Morse et al. 2004](#)). The clumpiness of the ejecta lead to variations in the reverse shock speed in both position and time. The shocks that propagate through the clumps are slowed because of the jump in density relative to the smooth ejecta, with $v_s(\text{clump}) \approx v_s(\text{smooth})/\chi^{1/2}$ (under the assumption of equal ram pressure) with the resulting speeds ranging from $\sim 100 - 350 \text{ km s}^{-1}$. Because of cooling, the shocks in the clumps slow as they go radiative. The overall evolution of the gas and dust can be seen in [Figure 3](#) where the density is shown (background color) as well as the dust grain positions.

When the reverse shock encounters the clumps that contain the dust grains, the clumps are compressed. The shocks that propagate into the clumps are radiative because of their high density and their high O abundance, which enhances their cooling. As a result, the clumps cool and are compressed as they are slowed. The grains then decouple fairly quickly as can be seen in [Figures 3](#) and especially [4](#). The first few of panels of [Figure 4](#) show how clumps get torn apart after being shocked.

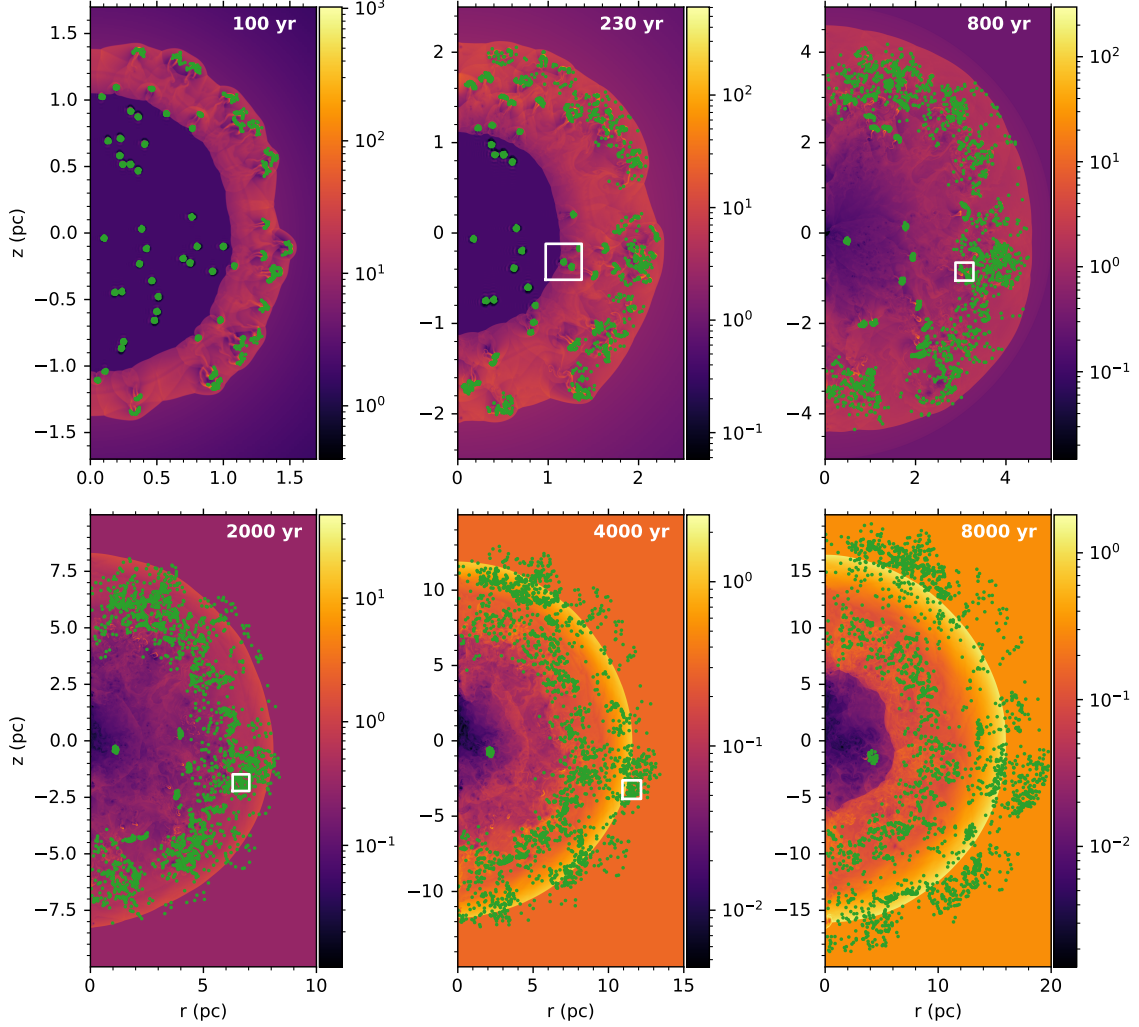


Figure 3. Time evolution of density and particle locations for a simulation that includes silicate grains initialized with a radius of $0.1 \mu\text{m}$. The background colors show the gas density (in cm^{-3} as indicated in the color bars) and the green dots indicate the grain positions. Note that the spatial and the density scales vary by as much as an order of magnitude between panels. The number of grains is the same in each panel, though at early times there is a lot of overlap of grains in clumps, which makes it appear that there are fewer grains. The white boxes in some panels show the sizes and positions of the panels at the corresponding times in the zoomed-in images of Figure 4. (Note however that there are more grains in the boxes here because some grains that originated in other clumps are included.)

The green dots in that figure show only the grains that started in a single clump of gas. In this figure the grains are silicate grains that have initial radii of $0.1 \mu\text{m}$ (as in Figure 3).

The grains are inertially sputtered on their way out of the clump due to their speed relative to the gas. The amount of mass lost in traversing a given column density is proportional to the grain cross section, so larger grains actually lose more mass than smaller grains, but it is a smaller fraction of the larger grain's mass. The

outer portions of the shocked clumps are hot, though cooler and denser than the shocked smooth ejecta. This leads to significant thermal sputtering of the grains in these transition regions. However, as the grains continue to move out through the remnant, their destruction rate slows because of the low density of the shock-heated smooth ejecta. This can be seen in Figure 5 where the mass evolution of each of the grains in Figure 4 is shown as a function of time. The sharp decline in the mass of the grains at $t = 200\text{--}300$ yr occurs as the shock passes through the clump, heating and decelerating it. As can be seen from the inset, different grains see the effects of the shock at different times because of their varying locations within the clump. Note that there is some sputtering before the shock hits because there is some leakage of grains near the clump edge out of the clump even before the shock hits it, which leads to motion relative to the clump and inertial sputtering. After the grains escape their clumps they propagate through the hot shocked smooth ejecta. While in the hot gas, they suffer thermal sputtering, which can be seen as the slow mass erosion in Figure 5 between $t \sim 500$ yr and ~ 3800 yr. The grains exit the remnant at $t \sim 3800$ yr and after that the sputtering rate decreases and is smoother as the grains are slowed in the ISM.

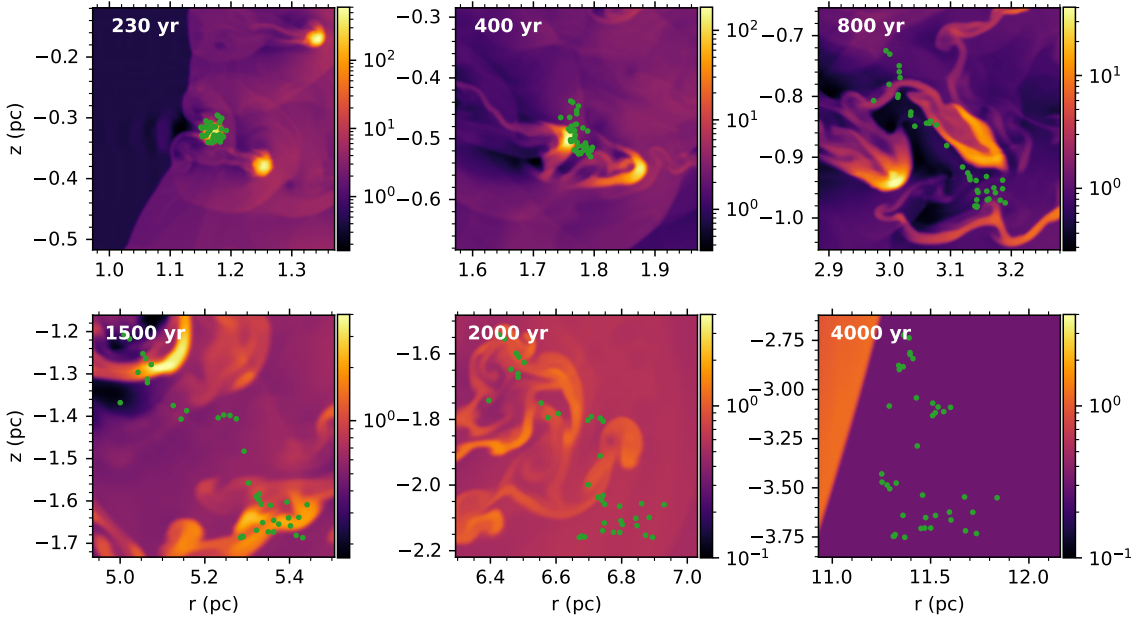


Figure 4. Zoomed in view of the evolution of grains that start in a single dense ejecta clump. This is from the same simulation as shown in Figure 3. Note the widely divergent paths taken by the grains after the clump has been destroyed by the passage of the reverse shock.

As discussed in §2.3, grain processing does not stop after escape ahead of the forward shock. The shock speed at the end of our 2D simulation ($t = 8000$ yr) is 870 km s^{-1} and its radius is 15.9 pc . Thus the grains that are already ahead of the shock must have averaged a radial speed of $\sim 2000 \text{ km s}^{-1}$, though grains still trapped in the

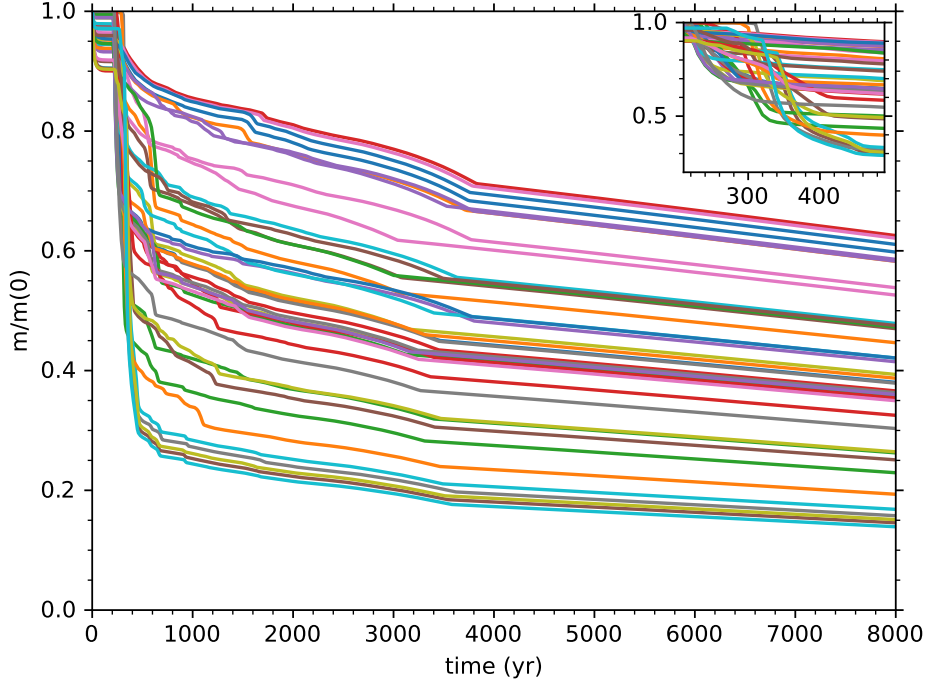


Figure 5. Grain mass evolution for grains in the clump shown in Figure 4. The grains lose most of their mass when the reverse shock passes through their ejecta clump at $t \sim 200\text{--}300$ yr. The inset shows a zoomed-in view of the time period when the shock is propagating through the clump. The spread in the destruction rates reflects the different times of encounters with the reverse shock caused by the different locations of the grains in the clump. The grains exit the remnant at $t \sim 3800$ yr. After that they are sputtered more slowly as they move through the ISM.

remnant have had lower average speeds. Indeed we find that even for grains as small as $0.1 \mu\text{m}$ the velocities at that time for grains ahead of the shock range from $\sim 800 \text{ km s}^{-1}$ to nearly 1400 km s^{-1} . Larger grains can have velocities up to $\sim 4000 \text{ km s}^{-1}$. As can be seen from Figure 6, this will lead to substantial further loss of mass as the grains slow in the ISM. Taking 1000 km s^{-1} as an example, a silicate grain will lose 64% of its mass as it slows and a carbonaceous grain will lose 44% of its mass.

Figure 6 also illustrates that there is a wide range of sputtered fractions for different grains depending on where in the remnant and even where within a clump the grain originated. In Figure 7 we show the grain size distributions that result for silicate grains that have initial sizes of $0.25 \mu\text{m}$. Note that all of the grains in these histograms started with the same grain size. The size distribution evolves toward smaller sizes over time while maintaining a similar shape. Unlike the interstellar grain size distribution, which is heavily weighted to small grain sizes (by number), these distributions are weighted to the large grain end. Of course the actual grain size distribution that is injected into the ISM will depend on the size distribution of the grains formed. The distributions shown indicate that the final distribution injected into the ISM will

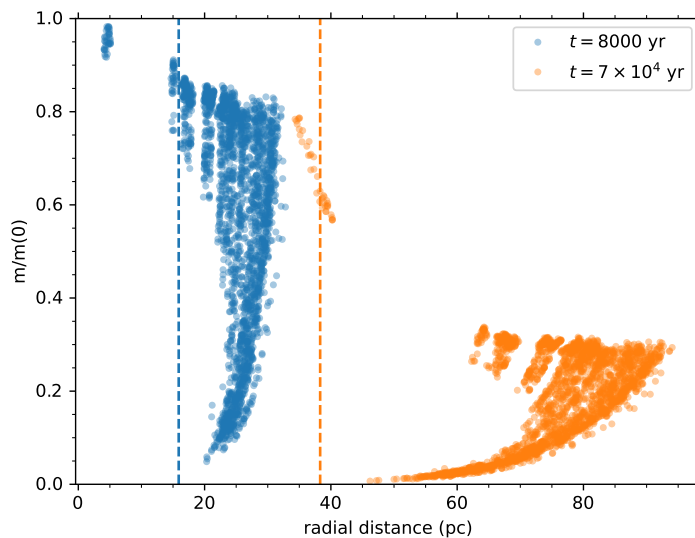


Figure 6. The evolution of grain mass for silicate grains with an initial radius of $0.25 \mu\text{m}$. The blue dots show the grain masses vs. radial distance at the end of the 2D simulation ($t = 8000 \text{ yr}$). The orange dots show the extrapolated evolution to a time $t = 7 \times 10^4 \text{ yr}$ after the explosion when the remnant is beginning to go radiative. The extrapolation is done by using the shock radius as calculated by a 1D simulation combined with Sedov-Taylor profiles for the density, temperature and velocity inside the remnant (see text). In this case nearly all of the grains are able to escape the remnant’s outer shock (shown as dashed lines at each time), though substantial mass loss has occurred between 8000 yr and $7 \times 10^4 \text{ yr}$. Further destruction occurs as the grains are slowed in the ISM.

Table 1. Grain Mass Survival Fraction

grain type initial size (μm)	silicate		carbonaceous	
	t_{sh}	t_{th}	t_{sh}	t_{th}
0.04	0.004	0.003	0.021	0.016
0.1	0.028	0.022	0.350	0.300
0.25	0.198	0.106	0.702	0.460
0.395	0.400	0.169	0.818	0.488
0.625	0.602	0.218	0.893	0.503

NOTE— $t_{sh} = 7 \times 10^4 \text{ yr}$ is the shell formation time for the remnant. t_{th} is the time at which the grain has slowed below the threshold speed for sputtering, $v_{th} \sim 20 \text{ km s}^{-1}$, which varies from grain to grain.

be similar to the initial distribution from grain formation, though shifted to smaller grain sizes and with an added tail toward the smaller grain size end.

We list the the final results of our calculations of the fraction of initial mass remaining for grains of different types and initial sizes in Table 1. We give both the

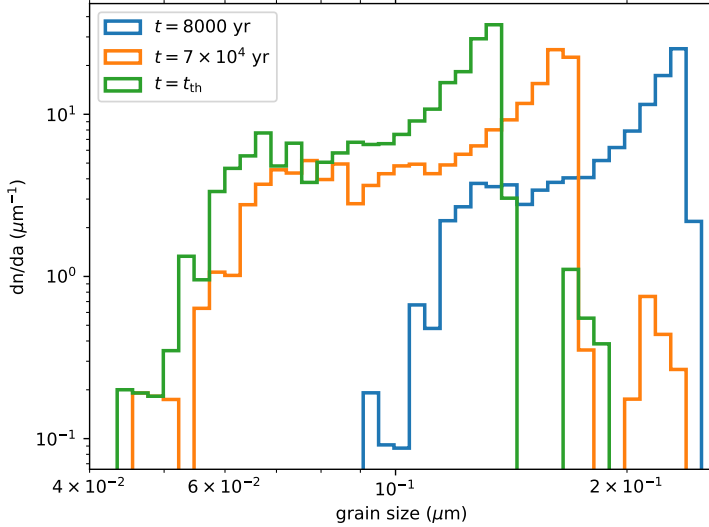


Figure 7. Grain size distributions for the case of silicate grains with initial size of $0.25 \mu\text{m}$. The histograms are normalized such that the integral over the distribution is 1 and use bins that are constant logarithmic intervals. We show the distributions from $t = 8000$ yr (the end of the 2D simulation), $t = 7 \times 10^4$ yr (the shell formation time) and t_{th} the time when the grains slow to below the sputtering threshold. The distribution shapes do not change very much even as the total remaining mass in the grains shrinks. Unlike the interstellar grain size distribution derived from observations, these are weighted toward the largest grain sizes. The actual size distribution injected into the ISM will depend on the initial size distribution of the grains formed in the ejecta clumps.

mass fraction of grains remaining at the end of the 1D simulation extrapolation (essentially the shell formation time for the remnant, $t_{\text{sh}} = 7 \times 10^4$ yr) and at the time t_{th} that each grain is slowed to the threshold velocity v_{thresh} for inertial sputtering. The threshold velocity for both silicate and carbonaceous grains is $\sim 20 \text{ km s}^{-1}$. It is clear that for the largest grain sizes the fraction of mass remaining is almost as much as would be expected if the grains had been directly released into the ISM at high speeds. Thus if even larger grains are formed in SNe, we expect their surviving mass fraction to be roughly the same as for the largest grains in the table.

To determine how much dust SNe can inject into the ISM, we need a few more pieces of information: the total mass that is condensed into grains and the grain size distribution for the grains formed. The mass of metals produced by SNe has been estimated in a number of studies. As an example, [Woosley & Heger \(2007\)](#) have calculated the mass of metals in the ejecta of the explosion of a star with initial mass $19 M_{\odot}$. Using their results, we calculate the maximum dust masses in the ejecta assuming that all the Mg, Si, Fe and $4/3$ of their combined number of O atoms were locked up in silicate dust of the form MgSiFeO_4 and that all the C was locked up in carbon dust. Doing this we find that the SN can produce $0.473 M_{\odot}$ of silicate grains and $0.209 M_{\odot}$ of carbonaceous grains.

Table 2. Overall Grain Mass Survival Fractions for Different Initial Size Distributions

size distribution ^a	silicate	carbonaceous
LN1	0.0316	0.348
LN2	0.128	0.470
LN3	0.208	0.501
PL1	0.0405	0.316
PL2	0.139	0.439
PL3	0.0702	0.317

^aThe grain size distributions are described in the text and shown in Figure 7 (solid lines). LN# are log-normal distributions and PL# are power-law distributions.

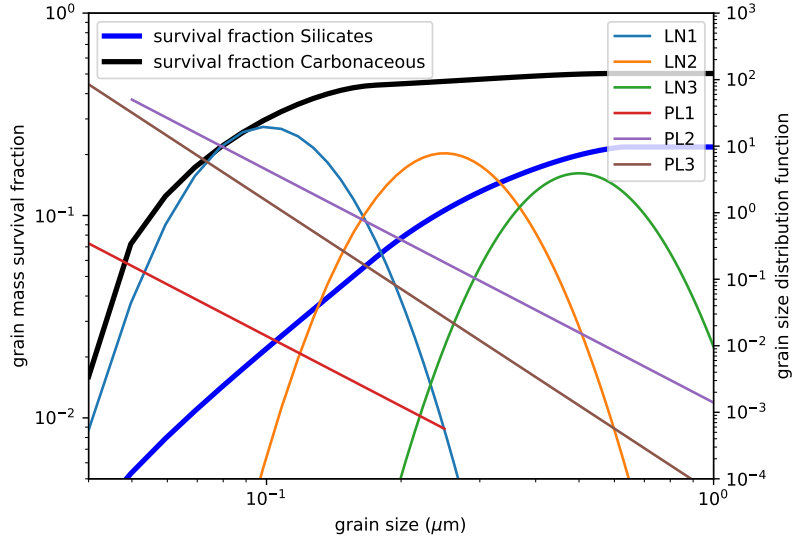


Figure 8. Dust mass survival fractions for silicate and carbonaceous grains (thick lines and left axis) and the grain size distributions we have examined (thin lines, right axis). The survival fractions are just those in Table 1 (each point calculated for a single grain size) with a quadratic spline interpolation. The parameters for the size distributions are detailed in the text. Note that for PL1 and PL2 the power laws extend to smaller sizes than shown in the plot. Such small grains are all destroyed inside the remnant, but are important to include for the overall normalization. The overall survival fraction is the survival fraction as a function of mass integrated over the initial mass distribution of the formed grains (i.e. the size distribution times the grain mass).

As for grain size distributions, the most comprehensive calculations of grain formation in the dense ejecta of SNe are from Sarangi & Cherchneff (2015) and Sluder et al. (2018). Neither work characterizes the size distribution in a simple way and such calculations are difficult and subject to a variety of uncertainties. Rather than attempt

to use their results then, we have chosen to use a couple of simple characterizations, namely a power law,

$$\frac{dn}{da} = \frac{1 + \gamma}{(a_{\max}^{1+\gamma} - a_{\min}^{1+\gamma})} a^{-\gamma}, \quad (8)$$

and a log-normal distribution,

$$\frac{dn}{da} = \frac{1}{a\sigma\sqrt{2\pi}} \exp\left(\frac{-(\ln(a/a_{\text{peak}}) - \sigma)^2}{2\sigma^2}\right), \quad (9)$$

where the distributions are normalized such that the integral of dn/da over the full size range is equal to unity. For the log-normal distribution the parameters are the grain size at the peak of the distribution, a_{peak} and the width parameter, σ . We have assumed that $\sigma = 0.2$ in all cases. For the power law distributions, we need to assume the minimum and maximum grain sizes, a_{\min} and a_{\max} , as well as the value of γ . The size distributions that we have examined are as follows:

- LN1: log-normal with peak at $0.1 \mu\text{m}$
- LN2: log-normal with peak at $0.25 \mu\text{m}$
- LN3: log-normal with peak at $0.5 \mu\text{m}$
- PL1: Mathis et al. (1977) style power law, $a_{\min} = 0.005 \mu\text{m}$, $a_{\max} = 0.25 \mu\text{m}$, $\gamma = 3.5$
- PL2: $a_{\min} = 0.05 \mu\text{m}$, $a_{\max} = 1.0 \mu\text{m}$, $\gamma = 3.5$
- PL3: $a_{\min} = 0.04 \mu\text{m}$, $a_{\max} = 1.0 \mu\text{m}$, $\gamma = 4.4$

These size distributions are illustrated in Figure 8 where the survival fractions from Table 1, interpolated by a quadratic spline, are also plotted. PL3 has the power law exponent that Sluder et al. (2018) find for their results, though the a_{\min} and a_{\max} values we have chosen do not match their results closely.

To calculate the overall fraction of grains that survive and are injected into the ISM, we need to integrate the mass distribution of grains over the grain mass survival fraction. The mass distribution is just the size distribution times the mass of a grain, $(4/3)\pi a^3 \rho_{\text{gr}}$, with proper normalization, where ρ_{gr} is the mass density of the solid grain material. We have carried out such calculations for the size distributions and the results are listed in Table 2. From these it is clear that any size distribution that has a large grain cutoff that is too small results in a small fraction of silicates grains surviving. Only the LN3 distribution leads to more than 20% survival. On the other hand, the relatively large fraction of even small carbonaceous grains that survive results in an overall survival fraction that is not highly sensitive to our assumed size distribution, with more than 30% survival in all cases and about 50% survival for distribution LN3. This is primarily due to the lower sputtering yield for carbonaceous grains, especially near the peak of the yield at $v \sim 500 - 1000 \text{ km s}^{-1}$.

The total effective mass of dust injected into the ISM is the product of the overall survival fraction, as listed in Table 2, and the total mass of dust (of the particular type) produced by the SN. If we take the values of $0.473 M_{\odot}$ for silicate dust and $0.209 M_{\odot}$ for carbonaceous dust as the maximum masses of dust that can be produced by a $19 M_{\odot}$ star, as referenced above, then the total mass of dust injected into the ISM is $0.098 M_{\odot}$ of silicate dust and $0.105 M_{\odot}$ of carbonaceous dust per SN. Here we have assumed the LN3 size distribution. Based on our calculations, this is essentially the maximum amount of dust that can be injected since this size distribution weights large grains that have close to a maximal mass survival fraction. Note that these values also assume 100% conversion of grain constituent elements in the SN into grains. Near total conversion into grains is supported by observations of SN 1987A (Matsuura et al. 2015) and Cas A (Barlow et al. 2010; Arendt et al. 2014). It is clear that less optimistic assumptions can lead to much smaller injection rates for silicate grains in particular. For carbonaceous grains, even a size distribution weighted toward smaller grains such as PL3 still allows for as much as $0.07 M_{\odot}$ of grain injection.

4. CONCLUSIONS

We have shown that dust grains formed in the dense ejecta of SNe can escape from the clumps and survive the reverse shock. The grains decouple from the gas and stream outward in the remnant. Grains that are large enough, $\sim 0.25 \mu\text{m}$ for silicates and $\sim 0.1 \mu\text{m}$ for carbonaceous grains, can escape ahead of the forward shock into the surrounding ISM. However, the grains must slow after reaching the ISM to be considered as contributing to the dust content of the medium, which entails further erosion via inertial sputtering. Including the sputtering while slowing sets the upper limit on the survival mass fraction of SN-created grains. For an initial grain mass distribution weighted toward large, $a \sim 0.5 \mu\text{m}$, grains, roughly 20% (by mass) of silicate grains and up to 50% of carbonaceous grains are injected into the ISM. Considering the case of a $19 M_{\odot}$ star, the amount of mass in the grain constituents in the SN leads us to expect at most about $0.1 M_{\odot}$ in either silicate or carbonaceous grains can survive injection into the ISM.

ACKNOWLEDGMENTS

This work has been supported by NASA Theory Program grant No. NNX17AH80G. We have benefited from the use of high performance computing resources of NASA's Pleiades cluster as well as the Smithsonian Institution's Hydra cluster. The code FLASH used in this work was in part developed by the DOE NNSA-ASC OASCR Flash Center at the University of Chicago. We thank Elisabetta Micelotta for helpful conversations.

Facilities: Smithsonian's Hydra cluster, NASA's Pleiades HPC cluster

Software: FLASH (Fryxell et al. 2000; Dubey et al. 2012, <http://flash.uchicago.edu/site/flashcode/>), python (Van Rossum & Drake Jr 1995), numpy (Oliphant 2006), scipy (Jones et al. 2001), yt (Turk et al. 2011), Cloudy (Ferland et al. 2017)

REFERENCES

- Arendt, R. G., Dwek, E., Kober, G., Rho, J., & Hwang, U. 2014, *ApJ*, 786, 55, doi: [10.1088/0004-637X/786/1/55](https://doi.org/10.1088/0004-637X/786/1/55)
- Baines, M. J., Williams, I. P., & Asebiomo, A. S. 1965, *MNRAS*, 130, 63
- Barlow, M. J., Krause, O., Swinyard, B. M., et al. 2010, *A&A*, 518, L138, doi: [10.1051/0004-6361/201014585](https://doi.org/10.1051/0004-6361/201014585)
- Bertoldi, F., Carilli, C. L., Cox, P., et al. 2003, *A&A*, 406, L55, doi: [10.1051/0004-6361:20030710](https://doi.org/10.1051/0004-6361:20030710)
- Bianchi, S., & Schneider, R. 2007, *MNRAS*, 378, 973, doi: [10.1111/j.1365-2966.2007.11829.x](https://doi.org/10.1111/j.1365-2966.2007.11829.x)
- Biscaro, C., & Cherchneff, I. 2016, *A&A*, 589, A132, doi: [10.1051/0004-6361/201527769](https://doi.org/10.1051/0004-6361/201527769)
- Bocchio, M., Marassi, S., Schneider, R., et al. 2016, *A&A*, 587, A157, doi: [10.1051/0004-6361/201527432](https://doi.org/10.1051/0004-6361/201527432)
- Cox, D. P., & Franco, J. 1981, *ApJ*, 251, 687, doi: [10.1086/159514](https://doi.org/10.1086/159514)
- Draine, B. T. 2009, in *Astronomical Society of the Pacific Conference Series*, Vol. 414, *Cosmic Dust - Near and Far*, ed. T. Henning, E. Grün, & J. Steinacker, 453. <https://arxiv.org/abs/0903.1658>
- Draine, B. T., & Salpeter, E. E. 1979a, *ApJ*, 231, 438, doi: [10.1086/157206](https://doi.org/10.1086/157206)
- . 1979b, *ApJ*, 231, 77, doi: [10.1086/157165](https://doi.org/10.1086/157165)
- Dubey, A., Calder, A. C., Daley, C., et al. 2012, *Int. J. High Perf. Comp. Appl.*, online publication, 1094342012464404
- Dwek, E. 1987, *ApJ*, 322, 812, doi: [10.1086/165774](https://doi.org/10.1086/165774)
- Dwek, E. 2005, in *American Institute of Physics Conference Series*, Vol. 761, *The Spectral Energy Distributions of Gas-Rich Galaxies: Confronting Models with Data*, ed. C. C. Popescu & R. J. Tuffs, 103–122, doi: [10.1063/1.1913921](https://doi.org/10.1063/1.1913921)
- Dwek, E., & Arendt, R. G. 1992, *ARA&A*, 30, 11, doi: [10.1146/annurev.aa.30.090192.000303](https://doi.org/10.1146/annurev.aa.30.090192.000303)
- Dwek, E., & Cherchneff, I. 2011, *ApJ*, 727, 63, doi: [10.1088/0004-637X/727/2/63](https://doi.org/10.1088/0004-637X/727/2/63)
- Dwek, E., & Scalo, J. M. 1980, *ApJ*, 239, 193, doi: [10.1086/158100](https://doi.org/10.1086/158100)
- Ferland, G. J., Chatzikos, M., Guzmán, F., et al. 2017, *RMxAA*, 53, 385. <https://arxiv.org/abs/1705.10877>
- Fesen, R. A., Zastrow, J. A., Hammell, M. C., Shull, J. M., & Silvia, D. W. 2011, *ApJ*, 736, 109, doi: [10.1088/0004-637X/736/2/109](https://doi.org/10.1088/0004-637X/736/2/109)
- Fry, B. J., Fields, B. D., & Ellis, J. R. 2020, *ApJ*, 894, 109, doi: [10.3847/1538-4357/ab86bf](https://doi.org/10.3847/1538-4357/ab86bf)
- Fryxell, B., Olson, K., Ricker, P., et al. 2000, *ApJS*, 131, 273
- Gall, C., Andersen, A. C., & Hjorth, J. 2011, *A&A*, 528, A14, doi: [10.1051/0004-6361/201015605](https://doi.org/10.1051/0004-6361/201015605)
- Gomez, H. L., Krause, O., Barlow, M. J., et al. 2012, *ApJ*, 760, 96, doi: [10.1088/0004-637X/760/1/96](https://doi.org/10.1088/0004-637X/760/1/96)
- Hollenbach, D., & Salpeter, E. E. 1971, *ApJ*, 163, 155, doi: [10.1086/150754](https://doi.org/10.1086/150754)
- Hoppe, P., Leitner, J., & Kodolányi, J. 2015, *ApJL*, 808, L9, doi: [10.1088/2041-8205/808/1/L9](https://doi.org/10.1088/2041-8205/808/1/L9)
- Jones, A. P., Tielens, A. G. G. M., & Hollenbach, D. J. 1996, *ApJ*, 469, 740, doi: [10.1086/177823](https://doi.org/10.1086/177823)
- Jones, A. P., Tielens, A. G. G. M., Hollenbach, D. J., & McKee, C. F. 1994, *ApJ*, 433, 797, doi: [10.1086/174689](https://doi.org/10.1086/174689)
- Jones, E., Oliphant, T., Peterson, P., et al. 2001, *SciPy: Open source scientific tools for Python*. <http://www.scipy.org/>

- Kirchschlager, F., Barlow, M. J., & Schmidt, F. D. 2020, *ApJ*, 893, 70, doi: [10.3847/1538-4357/ab7db8](https://doi.org/10.3847/1538-4357/ab7db8)
- Kirchschlager, F., Schmidt, F. D., Barlow, M. J., et al. 2019, *MNRAS*, 489, 4465, doi: [10.1093/mnras/stz2399](https://doi.org/10.1093/mnras/stz2399)
- Laming, J. M., & Hwang, U. 2003, *ApJ*, 597, 347, doi: [10.1086/378268](https://doi.org/10.1086/378268)
- Lee, J.-J., Park, S., Hughes, J. P., & Slane, P. O. 2014, *ApJ*, 789, 7, doi: [10.1088/0004-637X/789/1/7](https://doi.org/10.1088/0004-637X/789/1/7)
- Mathis, J. S., Rumpl, W., & Nordsieck, K. H. 1977, *ApJ*, 217, 425, doi: [10.1086/155591](https://doi.org/10.1086/155591)
- Matsuura, M., Dwek, E., Barlow, M. J., et al. 2015, *ApJ*, 800, 50, doi: [10.1088/0004-637X/800/1/50](https://doi.org/10.1088/0004-637X/800/1/50)
- McKee, C. F., Hollenbach, D. J., Seab, G. C., & Tielens, A. G. G. M. 1987, *ApJ*, 318, 674, doi: [10.1086/165403](https://doi.org/10.1086/165403)
- Micelotta, E. R., Dwek, E., & Slavin, J. D. 2016, *A&A*, 590, A65, doi: [10.1051/0004-6361/201527350](https://doi.org/10.1051/0004-6361/201527350)
- Morse, J. A., Fesen, R. A., Chevalier, R. A., et al. 2004, *ApJ*, 614, 727, doi: [10.1086/423709](https://doi.org/10.1086/423709)
- Nath, B. B., Laskar, T., & Shull, J. M. 2008, *ApJ*, 682, 1055, doi: [10.1086/589224](https://doi.org/10.1086/589224)
- Nozawa, T., Kozasa, T., & Habe, A. 2006, *ApJ*, 648, 435, doi: [10.1086/505639](https://doi.org/10.1086/505639)
- Nozawa, T., Kozasa, T., Habe, A., et al. 2007, *ApJ*, 666, 955, doi: [10.1086/520621](https://doi.org/10.1086/520621)
- Oliphant, T. E. 2006, *A guide to NumPy* (Trelgol Publishing USA)
- Sarangi, A., & Cherkneff, I. 2015, *A&A*, 575, A95, doi: [10.1051/0004-6361/201424969](https://doi.org/10.1051/0004-6361/201424969)
- Sarangi, A., Matsuura, M., & Micelotta, E. R. 2018, *SSRv*, 214, 63, doi: [10.1007/s11214-018-0492-7](https://doi.org/10.1007/s11214-018-0492-7)
- Silvia, D. W., Smith, B. D., & Shull, J. M. 2010, *ApJ*, 715, 1575, doi: [10.1088/0004-637X/715/2/1575](https://doi.org/10.1088/0004-637X/715/2/1575)
- . 2012, *ApJ*, 748, 12, doi: [10.1088/0004-637X/748/1/12](https://doi.org/10.1088/0004-637X/748/1/12)
- Slavin, J. D., Dwek, E., & Jones, A. P. 2015, ArXiv e-prints, <https://arxiv.org/abs/1502.00929>
- Sluder, A., Milosavljević, M., & Montgomery, M. H. 2018, *MNRAS*, 480, 5580, doi: [10.1093/mnras/sty2060](https://doi.org/10.1093/mnras/sty2060)
- Sutherland, R. S., & Dopita, M. A. 1993, *ApJS*, 88, 253, doi: [10.1086/191823](https://doi.org/10.1086/191823)
- Tielens, A. G. G. M., McKee, C. F., Seab, C. G., & Hollenbach, D. J. 1994, *ApJ*, 431, 321, doi: [10.1086/174488](https://doi.org/10.1086/174488)
- Turk, M. J., Smith, B. D., Oishi, J. S., et al. 2011, *ApJS*, 192, 9, doi: [10.1088/0067-0049/192/1/9](https://doi.org/10.1088/0067-0049/192/1/9)
- Van Rossum, G., & Drake Jr, F. L. 1995, Python tutorial (Centrum voor Wiskunde en Informatica Amsterdam, The Netherlands)
- Weingartner, J. C., & Draine, B. T. 2001, *ApJ*, 548, 296, doi: [10.1086/318651](https://doi.org/10.1086/318651)
- Weingartner, J. C., Draine, B. T., & Barr, D. K. 2006, *ApJ*, 645, 1188, doi: [10.1086/504420](https://doi.org/10.1086/504420)
- Willingale, R., Bleeker, J. A. M., van der Heyden, K. J., & Kaastra, J. S. 2003, *A&A*, 398, 1021, doi: [10.1051/0004-6361:20021554](https://doi.org/10.1051/0004-6361:20021554)
- Wolfire, M. G., McKee, C. F., Hollenbach, D., & Tielens, A. G. G. M. 2003, *ApJ*, 587, 278, doi: [10.1086/368016](https://doi.org/10.1086/368016)
- Woodsley, S. E., & Heger, A. 2007, *PhR*, 442, 269, doi: [10.1016/j.physrep.2007.02.009](https://doi.org/10.1016/j.physrep.2007.02.009)